



A novel finite element method for the wear analysis of cemented carbide tool during high speed cutting Ti6Al4V process

Yang Wang¹ · Honghua Su¹ · Jianbo Dai¹ · Shubao Yang²

Received: 14 November 2018 / Accepted: 15 April 2019 / Published online: 27 April 2019
© Springer-Verlag London Ltd., part of Springer Nature 2019

Abstract

In the present research, three typical cutting tool wear mechanisms (abrasive wear, adhesive wear, and diffusive wear) were taken into consideration in the FE simulation of cutting tool with a specific user-defined subroutine. Based on the influence of temperature on the cutting tool wear form, a novel wear rate model was built integrating Usui, Takeyama, and Attanasio wear rate equation. The high-speed cutting tests were carried out on Ti6Al4V to determine the proposed wear rate model constant. The cutting forces and rack face wear morphologies obtained from FE simulation match well with those from experimental cutting tests. Finally, the effect of cutting parameters on tool wear was studied by FEM. The simulation results show that the impact of the cutting speed on the cutting tool life is more significant than that of feed rate, and the preferred ranges of cutting speed and feed rate for extending cemented carbide cutting tool in high-speed dry cutting Ti6Al4V are 90–150 m/min and 0.10–0.20 mm/r, respectively.

Keywords Cutting tool wear · Wear rate model · FE simulation · High speed cutting

1 Introduction

Recently, the titanium alloy has been widely used in the aerospace industry due to superior physical and chemical properties [1, 2], such as low density, corrosion resistance, high strength, good low-temperature resistance, high temperature resistant [3–6]. The inherent disadvantages (low thermal conductivity, high chemical activity, and low elastic modulus) make the titanium alloy a typical difficult-to-machining material [7–9]. High-speed cutting is the key technology for realizing high efficiency machining for this kind difficult-to-machining titanium alloy. However, the rapid wear of the cutting tool has become an obstacle to further improving the machining efficiency and quality of these titanium alloy materials.

Tool wear is an important aspect of the difficult-to-machining materials cutting process, which has a significant impact on the component quality, chip formation, and the costs of the cutting process. Enormous efforts have been made on the cutting tool wear mechanisms. Costes [10] studied the mechanism of tool wear in cutting Inconel 718 process. Through SEM and chemical analysis, he concluded that the cutting tool failure was mainly caused by abrasive, adhesive, and diffusive wear in the cutting process. Takeyama and Murata [11] believed that mechanical wear and diffusive wear effects should be considered in tool wear. Mathew [12] and Attanasio [13] found that when the cutting temperatures are below 700 °C, the cutting tool wear form includes abrasive wear and adhesive wear, and once the temperatures exceed 700 °C, the diffusive equation becomes the main wear form. Generally, during the high-speed cutting process, the cutting tool wear occurs in the form of the combination of those wear mechanisms, which is mainly influenced by the cutting temperatures.

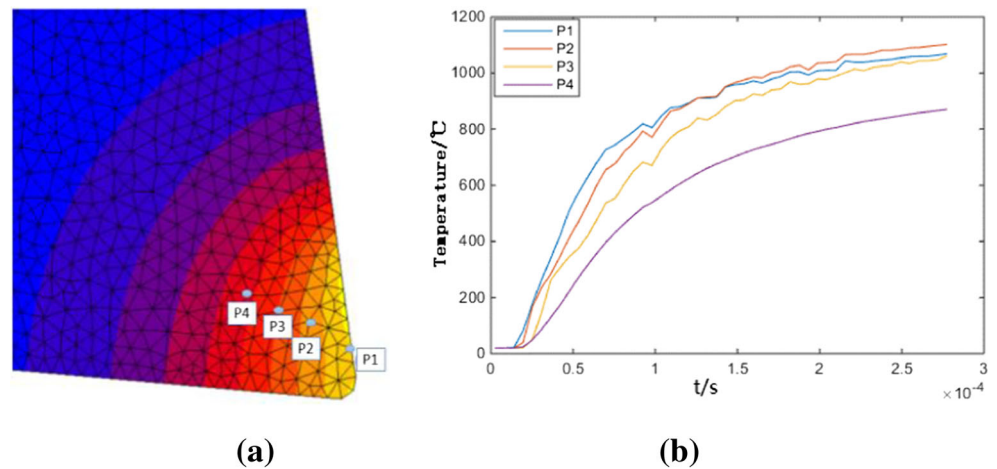
To improve the cutting efficiency and quality of titanium alloy and prolong the cutting tool life, the accurate prediction of tool wear in high-speed cutting of titanium alloys has become a popular topic. Compared with the empirical formula and theoretical calculation, numerical simulation is a cost-effective method for the cutting tool prediction, which was

✉ Honghua Su
shh@nuaa.edu.cn

¹ College of Mechanical and Electrical Engineering, Nanjing University of Aeronautics and Astronautics, Nanjing 210016, People's Republic of China

² College of Mechanical Engineering, Anhui University of Technology, Maanshan 243000, People's Republic of China

Fig. 1 Tool temperature changes over time



widely used to study the various aspects of the machining process, such as surface integrity [14], chip breakage [15], tool wear, or dimension deviation caused by thermal elastic deformation [16, 17]. Attanasio et al. [18] built a 3D numerical model for predicting the tool wear in metal cutting operations considering the diffusive wear mechanism through a specific subroutine. Filice et al. [19] proposed an effective FE model able to model both flank and crater, and discussed the limits of numerical simulations as concerns thermal aspects; they proposed the way that increase the heat transfer coefficient “ h ” between tool and chips, quickly obtaining stable temperature field. Binder et al. [20] introduced the thermos-mechanical load to calculate the local adhesive wear rates and modify the tool geometry accordingly with a wear subroutine. However, as described above, the tool wear mechanisms involved in the high-speed cutting titanium alloys include abrasive, adhesive, and diffusive wear, which may be the main reason for the unpredictable error between the experimental

and numerical results. Hence, it is highly necessary to implement a novel wear rate model, able to take into account the abrasive, adhesive, and diffusive wear mechanisms, into FEM simulation of high-speed cutting titanium alloy process through a specific subroutine.

The present work is devoted to building a reliable FE model of tool wear that can consider various wear mechanisms (abrasive wear, adhesive wear, diffusive wear) occurring in high-speed cutting Ti6Al4V process. A novel technique is introduced to update the wear geometry of the cutting tool by the user subroutine without manual intervention of the numerical simulation. The validity of the model is verified through experiments. The carbide tool life and wear morphology in the titanium alloy machining process was predicted by FEM, and the model predicts the location and depth of actual tool wear. The reasonable range of cutting parameters was determined, which provides important information for improving the machining efficiency and reducing cost.

Fig. 2 Simulation sequence conducted for every discrete time step Δt_{wear} in wear simulation

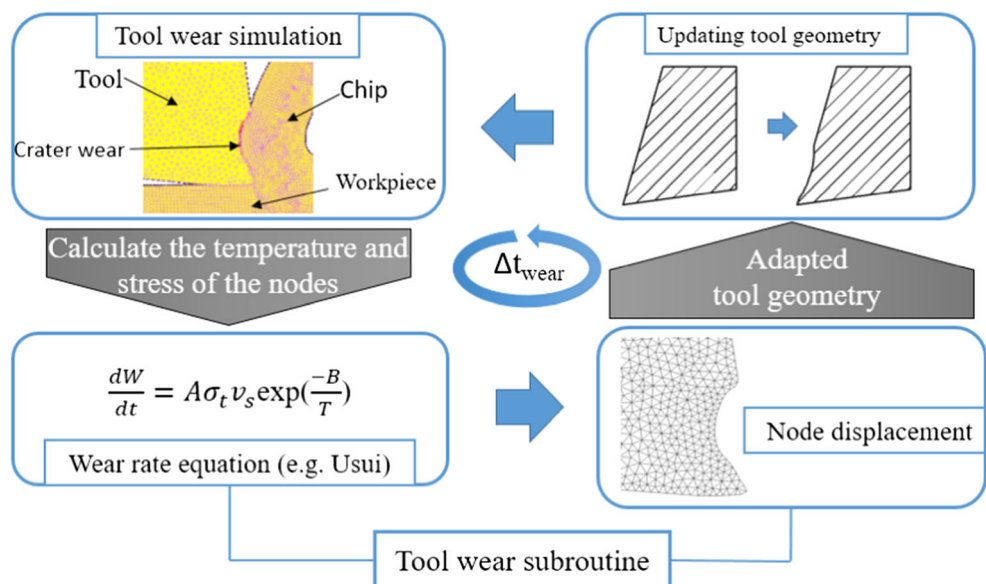
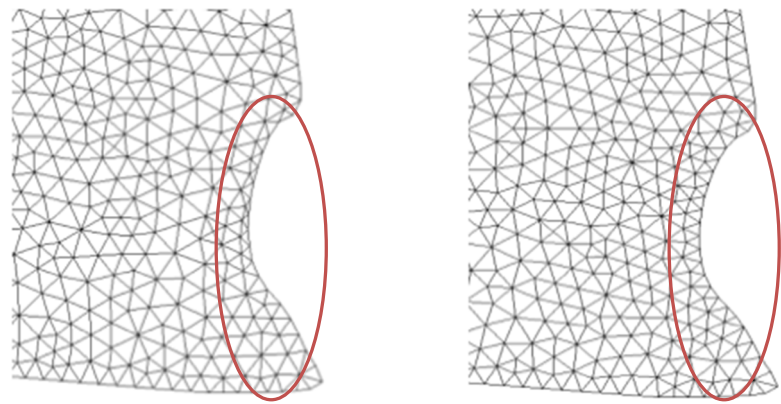


Fig. 3 The comparison of tool morphology before and after remeshing. **a** Before remeshing, **b** After remeshing



(a) Before remeshing

(b) After remeshing

2 Implementation of the tool wear simulation

In the actual cutting test, a cutting tool life may last from several seconds to hours or even weeks, and there is a big contrast between the machining time required for reaching thermal steady state conditions (usually about 10–20 s). However, the machining time in the 2D simplified cutting process simulation model just is of the order of 10^{-3} , which makes it almost impossible to realize a simulation of the entire tool life due to the tremendous computing times. Hence, the continuous progress of wear is discretized into finite steps for the purpose of tool wear simulation.

The continuous progress of tool wear was approximated by discretizing the cutting time in intervals. For each interval, the tool wear simulation mainly focuses on the steady-state cutting operations in continuous chip formation with reasonable constant loads (pressure, temperature, sliding velocity, etc.).

In order to reach the steady state in each discrete step, especially in the thermal aspects, some alternatives have been proposed [21, 22]. Relevant importance is assumed by increasing the global heat transfer coefficient “ h ” at the tool-chip interface. Generally, considering the larger value of the above coefficients, it is assumed that there are more effective heat transfer conditions at the chip-tool interface. In this paper, a large heat transfer coefficient h is $2000 \text{ kw/m}^2\cdot\text{K}$ is adopted,

which causes a large amount of heat to transfer to the tool in a short time, so that it can reach the thermally stable state rapidly. As shown in Fig. 1a, the temperature distribution of the tool is obtained after increasing the heat transfer coefficient, and four points (P1, P2, P3, P4) from the surface of the tool to the interior can be used to see the temperature change in the cutting process; the tool temperature quickly (10^{-4} s) reaches the steady state as shown in Fig. 1b.

2.1 Procedures of tool wear simulation

The process of tool wear simulation in each discrete cutting time (Δt_{wear}) is depicted in Fig. 2. The assumption of the underlying approach is to calculate the wear rates in a discrete point t_i , and between these points, it is assumed that the temperature field and the stress field are not affected by the change of the tool wear, and the wear rate of the tool is assumed to be constant. The time interval between two consecutive points t_i and t_{i+1} is introduced as Δt_{wear} . For every discrete time, step is simulated. First, in the simulation, local temperature, stress, and sliding velocity for the tool are transmitted to the user-defined tool wear subroutine. Then, in the subroutine, the local tool wear rate is calculated according to the tool wear rate equation. Since tool wear is not only to be calculated, but also to be realized in the tool geometry, the local tool wear rate

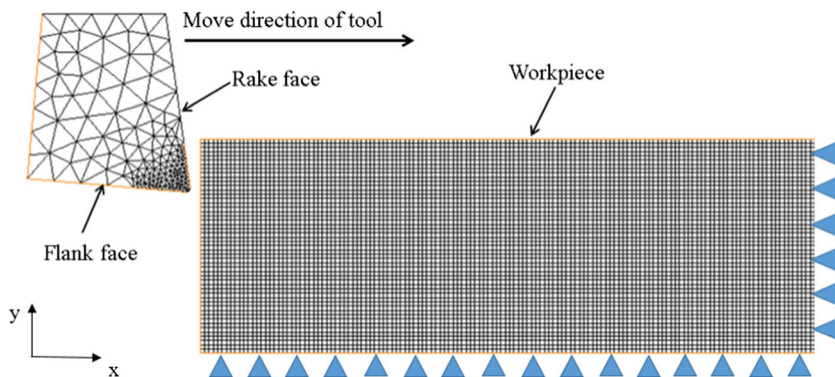
Table 1 Material parameters for cemented carbide [23]

Temperature (°C)	20	200	400	600
Ultimate strength (MPa)	2600	2550	2350	2000
Young’s modules (GPa)	580	570	560	540
Density (kg/m^3)	14,500			
Thermal expansion (10^{-6} K^{-1})	5.4	5.4	5.4	5.6
Heat capacity (J/kg·K)	220	240		
Thermal conductivity (W/m·K)	90			
Poisson’s ration	0.22			

Table 2 Johnson–Cook’s law parameters and their values

Parameter	Value
A	553.1
B	600.8
C	0.0134
n	0.234
m	1
$\bar{\epsilon}_0^-$	1
T_{room} (K)	293.15
T_{melt} (K)	1733

Fig. 4 Finite element geometry model of orthogonal cutting



is converted into the node displacement of each tool node. Finally, the tool morphology is updated. This procedure continues iteratively until the total cutting time is reached.

During the tool wear simulation process, if the interior of the tool model mesh does not have a corresponding adjustment, it will lead to excessive distortion of the elements and the uneven surface section of the tool after wear, which will affect the convergence of the cutting process. This paper used the strong automatic remeshing function in finite element software to adjust the internal meshes of the tool to ensure the smoothness of the tool surface.

According to the specification of the elements and the tool wear rate in the simulation model, this paper establishes the corresponding remeshing criterion. The elements on the tool are remeshing every 20 incremental steps. The comparison of tool morphology before and after remeshing is shown in Fig. 3. It can be seen that Fig. 3a is the tool wear morphology before remeshing, and after the remeshing, the tool wear morphology is more smooth, as shown in Fig. 3b.

2.2 Finite element model of tool wear

2.2.1 Materials model

The simulation consists of two objects, the tool and the workpiece, which are set as elastic-plastic bodies. The uncoated WC–Co carbide tools (92% WC, 8% Co) are the Kenna 313. The material parameters for the tool at different temperatures are specified in Table 1 [23]. The flow stress of the work material Ti6Al4V is calculated by the Johnson–Cook (J–C) constitutive equation considering strain hardening, strain-rate hardening, and thermal softening [13, 24]. The Johnson–Cook model selected in this paper is expressed as:

$$\bar{\sigma} = \left(A + B\bar{\epsilon}^n \right) \left(1 + C \ln \frac{\dot{\bar{\epsilon}}}{\dot{\bar{\epsilon}}_0} \right) \left[1 - \left(\frac{T - T_{\text{room}}}{T_{\text{melt}} - T_{\text{room}}} \right)^m \right] \quad (1)$$

where A, B, C, m, n are the material constants of the Johnson–Cook constitutive equation, T is the local temperature, T_{room} is the reference value of the temperature, T_{melt} is the melting

temperature, $\bar{\epsilon}$ is the equivalent plastic strain, $\dot{\bar{\epsilon}}$ is the equivalent strain rate, and $\dot{\bar{\epsilon}}_0$ is the reference value of the strain rate. The adopted model constants are listed in Table 2.

2.2.2 Two-dimensional FE model

The 2D orthogonal cutting finite element model is shown in Fig. 4. The nose radius, rake angle, and flank angle of the cutting tool are 0.8 mm, 5°, and 8°, respectively. The cutting tool has 241 elements, and the mesh refinement is carried out on the cutting area, which can reduce the computational cost. The size of the Ti6Al4V workpiece is 2 mm × 0.8 mm, which is divided into 21,000 elements. In the simulation, the tool moves along the X -axis with the cutting speed of v m/min, and the bottom of the workpiece is fixed. The initial temperature of the workpiece and cutting tool is 20 °C, and the effect of convection heat transfer with the environment is neglected. The friction coefficient was 0.32 to simulate the low friction condition between the cutting tool and workpiece [25]. The simulation parameters are listed in Table 3, and the cutting depth is set to a fixed value of 1 mm.

2.3 Tool wear rate equation

In the present research, the abrasive wear, adhesive wear, and diffusive wear are taken account into the proposed wear model. The corresponding wear rate models of different tool wear forms are listed in Table 4, respectively. In the proposed wear rate model, it is assumed that there is no interrelationship between the different tool wear forms and no abnormal wear

Table 3 The parameters of the cutting simulation

Cutting parameters	Numeric value
Cutting speeds v (m/min)	90, 120, 150, 200, 250, 300
Cutting depth a_p (mm)	1
Feed rate f (mm/r)	0.1, 0.15, 0.2
Cooling mode	Dry machining

Table 4 Tool wear rate models [18]

Types of tool wear	Models of tool wear rate	Comments
Abrasive wear [11]	$\frac{dW_r}{dt} = Gv$	G is the constant, $G = 2.37 \times 10^{-11}$ v is the cutting speed, t is cutting time.
Adhesive wear [26]	$\frac{dW_a}{dt} = A\sigma_t v_s \exp\left(\frac{-B}{T}\right)$	v_s is the relative sliding velocity, σ_t is the normal stress on the contact surface of cutter and chip, T is the cutting temperature, A and B are the material constants.
Diffusive wear [13]	$\frac{dW_d}{dt} = D \exp\left(-\frac{E}{RT}\right)$	E is the activation energy in the diffusive process, R is the gas constant, D is the function of temperature: $D(T) = aT^3 + bT^2 + cT + d$. $a = 1.637 \times 10^{-9}$, $b = -5.5373 \times 10^{-6}$, $c = 6.1161 \times 10^{-3}$, $d = -2.251$

(breakage, chipping edge, crack) occurring in the whole cutting process. The total wear rate model considering the abrasive, adhesive, and diffusive wear could be calculated by [14]:

$$W = W_r(L, \sigma_a) + W_a(t, T) + W_d(t, T) \tag{2}$$

where W is the total wear, W_r is the abrasive wear, W_a is the adhesive wear, W_d is the diffusive wear.

The cutting temperature, a key factor influencing the wear forms occurring, was introduced in the total wear rate model. Many literatures [12, 13] demonstrate that when the temperature is below 700 °C, the tool wear form of the cemented carbide tool is mainly the combination of abrasive wear and adhesive wear, and once the temperature exceeds 700 °C, the tool wear form changes into the combination of adhesive wear and diffusive wear. The tool

wear rate model considering the abrasive, adhesive, and diffusive wear could be calculated by:

$$\begin{cases} \frac{dW}{dt} = Gv + A\sigma_t v_s \exp\left(\frac{-B}{T}\right) & T \leq T_d \\ \frac{dW}{dt} = A\sigma_t v_s \exp\left(\frac{-B}{T}\right) + D(T) \exp\left(\frac{-E}{RT}\right) & T \geq T_d \end{cases} \tag{3}$$

In addition, the applied adhesive wear equation has two constants A and B that need to be calibrated for a certain combination of material-cutting material.

2.4 Tool wear subroutines

The function of the user-defined subroutines is to extend the functions of the software by self-defined methods. The subroutines for finite element analysis software Marc are written in Fortran. The subroutine used for tool wear simulation is called “uwearindex” and enables the programmer to use a wide set of internal variables. The implemented routines are called and executed after every simulation step in the simulation.

Figure 5 gives an overview of the processes executed in the user subroutine. First, the tool temperature and stress in discrete time are calculated by the simulation. Then, the user-defined subroutine reads these parameters of the node on the tool surface in real time, determines whether the temperature reaches T_d , determines the form of tool wear, calculates the

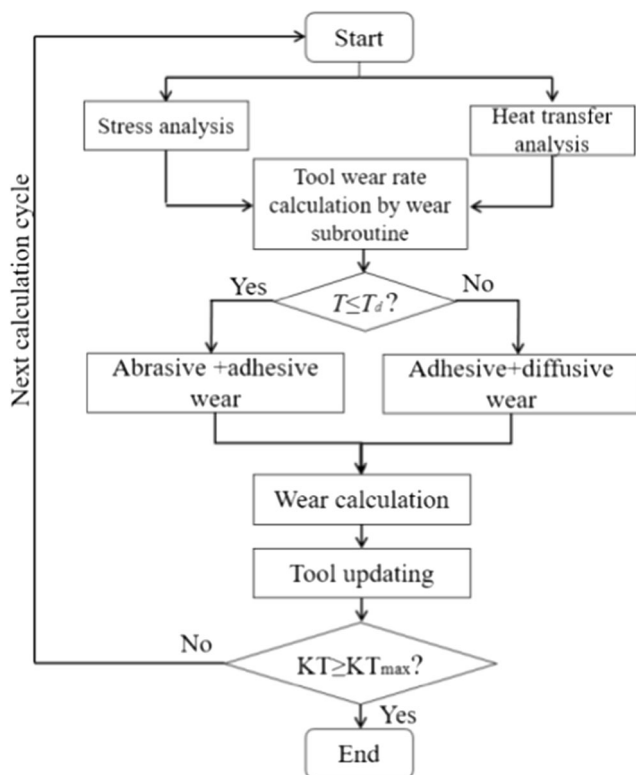


Fig. 5 The processes executed in the user subroutine

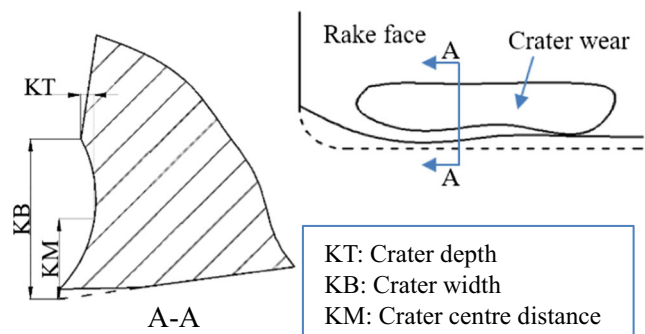
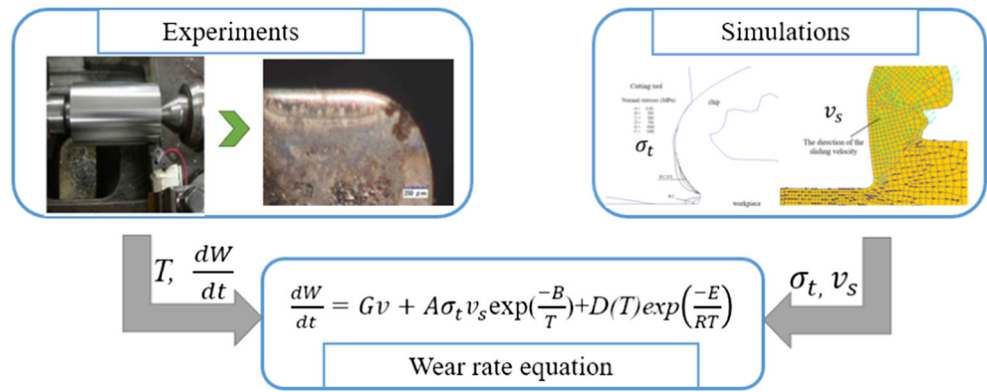


Fig. 6 Schematic diagram of the tool crater wear

Fig. 7 The process of determining the parameters of the tool wear rate model



nodal displacement, and updates the tool geometry based on wear rate equation. Finally, the amount of the tool wear obtained at different Δt_{wear} is superimposed to achieve the simulation of the whole tool wear process. If the tool wear is not up to the critical value of KT_{max} , then cycling the above steps is continued until the tool fails. According to international standard ISO3685-1977(E), the tool failure of carbide tool is recommended: $KT_{\text{max}} = (0.06 + 0.3f)$ mm, where f is the feed rate, and $KT_{\text{max}} = 0.1$ mm is set as the critical value of tool failure in this paper. As displayed in Fig. 6, the parameters of crater depth (KT), crater width (KB), and crater center distance (KM) were introduced to describe the crater wear condition of the rake surface.

3 Calibration of the tool wear rate equation

The proposed tool wear rate model has two constants A and B that need be calculated for a certain combination of cemented carbide tool and Ti6Al4V workpiece. The constants are determined by a hybrid approach using the above 2D orthogonal cutting FE model to obtain the normal stress and relative sliding velocity on the tool-chip interface and cutting experiments to attain the corresponding wear rate and the cutting temperature T , as displayed in Fig. 7.

3.1 Experimental setup

All the cutting experiments were carried out on the CA6140 turning lathe without coolant. The material of workpiece chosen for this study was Ti6Al4V alloy, which consisted of equiaxed α phase and β transformed microstructure. The detailed information about the chemical Ti6Al4V alloy is shown in Table 5. The material of KENNA K313 tool is uncoated

Table 5 The main chemical composition of the Ti6Al4V alloy [8]

Elements	Ti	Al	V	C	Fe	O	N
Content (%)	Bal.	5.5~6.8	3.5~4.5	0.08	0.3	0.2	0.05

WC–Co carbide, with the nose radius of 0.8 mm, rake angle of 5° , and flank angle of 8° .

As shown in Fig. 8, the temperature of the cutting tool is measured by the tool-work (dynamic) thermocouple [27] in the experiments. The technique is based on the thermo-electric effect that the different materials (tool and workpiece) generate an electric potential difference between cold junction B and the hot junction A in the closed loop. In the present cutting process, the hot junction A is the area of contact between the tool and the workpiece and the cold junction B is formed by the remote sections of the tool and the workpiece, connected by lead wires. The temperature value can be obtained according to the corresponding relationship between the measured electromotive force and the temperature in the thermocouple calibration system. The details of the experimental condition are listed in Table 6.

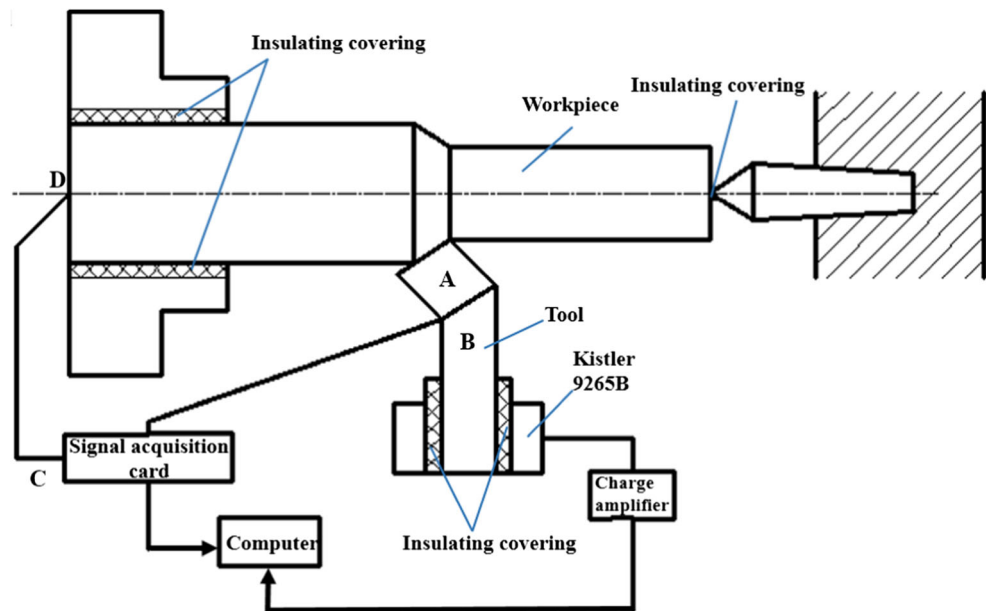
The single factor experiment method was used in the present cutting experiments. The cutting speed v and the feed rate f were changed respectively to analyze the influence of these two parameters on tool wear. The process parameters used for the experiment are listed in Table 7.

3.2 Determination of tool wear rate equation coefficient

As shown in Figs. 7 and 8, on the one hand, cutting experiments were conducted in section 3.1, the cutting temperature T of the cutting tool was measured, the depths of the crater wear of the tools were tracked with the 3D microscope Hirox KH7700, as shown in Table 8, and the wear rate (tool wear per unit time) was calculated.

On the other hand, as shown in Fig. 9, the measured tool wear morphology was imported into AutoCAD to reconstruct the tool geometry model manually, the calculation results of the previous step were taken as boundary conditions, and the simulation is continued with the worn tool to obtain the normal stress and relative sliding velocity for the corresponding time. The friction behavior of the tool-chip interface and the material constitutive model are consistent as shown in section 3.3. As shown in Fig. 10a, b, the average value of the cutting

Fig. 8 The schematic diagram of tool wear experiment



force signals measured by the experiments and simulations is taken as the cutting force, the main cutting force F_x as the research object in this paper. The accuracy of the simulation model was proved by comparing the cutting force obtained from the experiments with the simulation results. As shown in Fig. 10c, the cutting force obtained by the two methods has a similar trend with the change of cutting speed. After comparison, it is found that the maximum error between the experimental results and the simulation results does not exceed 8%, indicating that the simulation model is accurate. Finally, the normal stress σ_t and relative velocity v_s were obtained from the post-processing files. Substitute the formula for fitting, and obtain the specific value of A and B for $A = 4.8 \times 10^{-3}$, $B = 8500$. Substituting A and B values into Eq. (3), the total wear rate model considering the abrasive, adhesive, and diffusive wear could be calculated by:

$$\begin{cases} \frac{dW}{dt} = Gv + 4.8e^{-3}\sigma_tv_s \exp\left(\frac{-8500}{T}\right) & T \leq T_d \\ \frac{dW}{dt} = 4.8e^{-3}\sigma_tv_s \exp\left(\frac{-8500}{T}\right) + D(T) \exp\left(\frac{-E}{RT}\right) & T \geq T_d \end{cases} \quad (4)$$

Table 6 The experimental conditions

Machine tool	CA6140 turning lathe
Cutting tool	Kenna K313
Workpiece	Ti6Al4V, $\varphi 65$ mm, length 240 mm
Microscopy	Hirox KH7700
Dynamometer	Kistler 9265B
Charge amplifier	Kistler 5059A
Signal acquisition card	NI USB-6008

4 Experimental validation and numerical results

4.1 Validation of tool wear model

Figure 11 shows the tool wear mode and the morphology of the cutting tool at different moments when the cutting speed is 120 m/min, the feed rate is 0.1 mm/r, and the cutting depth is 1 mm. In the initial wear stage, the tool wear part mainly occurs at the tip of the tool, and the wear form of the rake face is characterized as the broad crater at the end of tool wear. As the cutting process is carried out, the depth and the width of the crater wear are increased. At 4 min, the KT value has reached 0.041 mm, while at 7.5 min, the tool KT value has reached 0.1 mm and the tool fails.

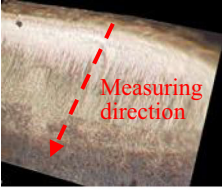
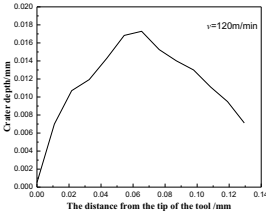
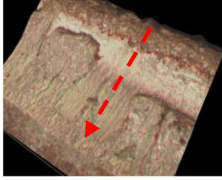
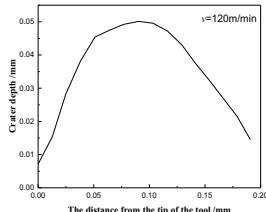
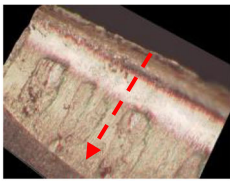
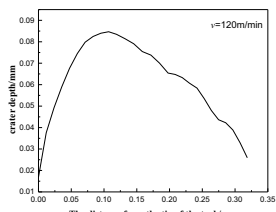
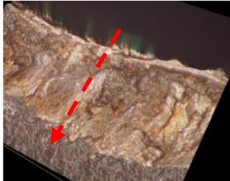
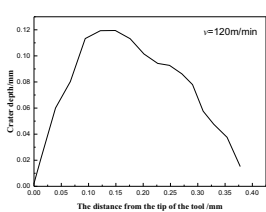
Hirox KH7700 was used to track the crater wear of the rake face of the tools in the experiments. The tool wear mode and the morphology of the cutting tool at different moments are shown in the Table 8; the cutting speed is 120 m/min, and the feed rate is 0.1 mm/r and the cutting depth is 1 mm.

Figures 12 and 13 show the tool wear experimental results compared with the simulation results. When the

Table 7 Process parameters for cutting experiment

Machining conditions	Parameter value
Cutting speeds v (m/min)	90, 120, 150
Cutting depth a_p (mm)	1
Feed rate f (mm/r)	0.1, 0.2
Cooling condition	Dry machining

Table 8 Change of tool wear quantity at different times in the experiments ($v = 120$ m/min)

Cutting time	Crater wear	Depths of the crater wear
2min		
4min		
6min		
8min		

cutting speed is 120 m/min, the feed rate is 0.1 mm/r, and cutting depth is 1 mm, the simulation values with the experimental values in the same change trend. In general, the difference between the simulation estimate and the measured value is small, and the error is less than 15%. It is shown that the simulation can reflect the actual wear process of the tool and fully verifies the effectiveness of the tool wear simulation model.

4.2 Analysis of the numerical results of tool wear

4.2.1 Impact of cutting speed on tool wear

Cutting speed is the most active factor affecting tool wear in all cutting parameters and the increase of cutting speed will lead to the increase of the cutting temperature, which will advance the adhesive wear and diffusive wear. The depth of crater wear KT (on the rake face of the cemented carbide tool) against the time under different cutting speeds is shown in

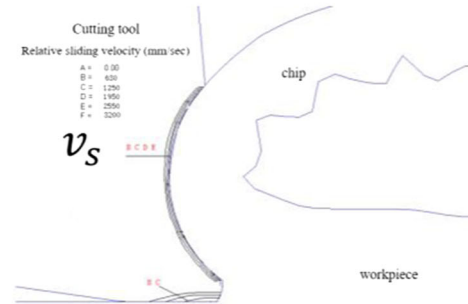
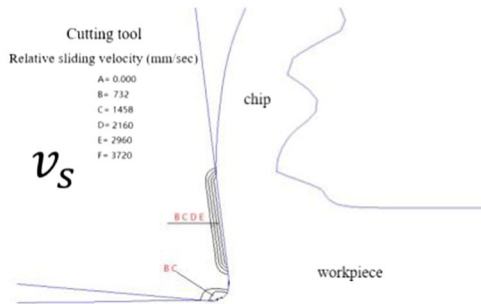
Fig. 14. As the cutting speed increases, the slope of the tool wear curve increases sharply, and the time needed to reach wear dulling standard ($KT = 0.1$ mm) is also getting shorter and shorter, indicating that the tool life will decrease with the increasing speed. For example, when the cutting speed is 90 m/min, the time required to meet the wear dulling standard of the tool rake face is 13.5 min. However, if the speed is increased to 120 m/min, the time required to meet the wear dulling standard of the tool rake face is 13.5 min; when the speed is increased to 150 m/min, the time is 5 min; when the cutting speed is increased to 200 m/min, 250 m/min, and 300 m/min, the curve in the graph rises in a straight line, and the cutting tool reaches the wear dulling standard within 2 min.

The simulation results show that the crater wear on the rake face is predominant under high-speed cutting of Ti6Al4V. The variances of the depth of crater wear with the distance from the tip of the tool under the different cutting speed are illustrated in Fig. 15. For example, as shown in Fig. 15a, under the



(a) Normal Stress distribution of the tool (KT=0)

(b) Normal Stress distribution of the tool (KT=0.05)

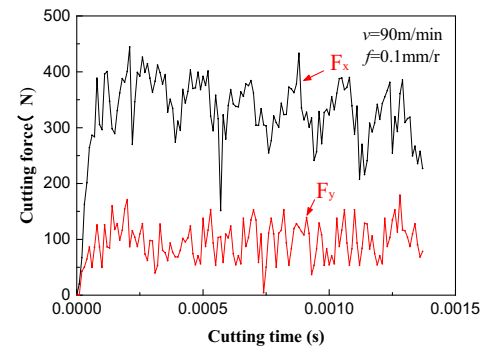
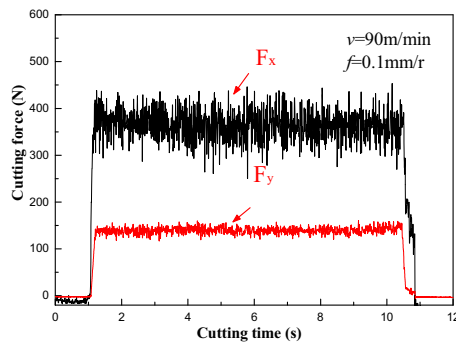


(c) Relative sliding velocity distribution (KT=0)

(d) Relative sliding velocity distribution (KT=0.05)

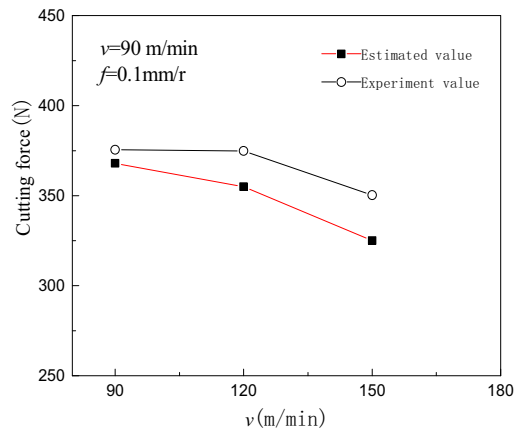
Fig. 9 The distribution of the normal stress and relative sliding velocity of the tool. **a** Normal stress distribution of the tool (KT = 0). **b** Normal stress distribution of the tool (KT = 0.05). **c** Relative sliding velocity distribution (KT = 0). **d** Relative sliding velocity distribution (KT = 0.05)

Fig. 10 Cutting force verification. **a** Experimental cutting force at $v = 90$ m/min. **b** Simulated cutting force at $v = 90$ m/min. **c** Comparison between experiments and estimated value



(a) Experimental cutting force at $v=90$ m/min

(b) Simulated cutting force at $v=90$ m/min



(c) Comparison between experiments and estimated value

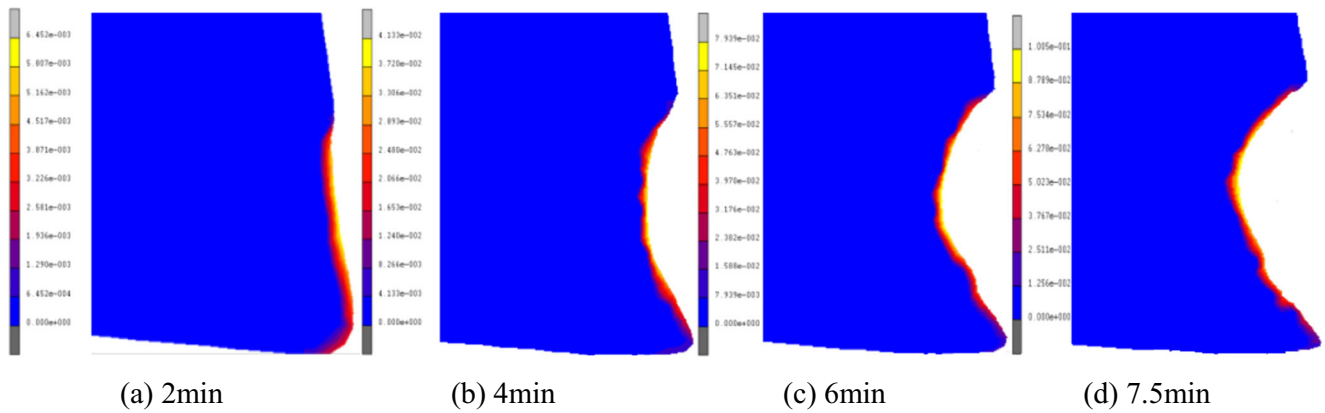


Fig. 11 Change of tool wear quantity at different times in the simulations ($v = 120$ m/min) **a** 2 min, **b** 4 min, **c** 6 min, and **d** 7.5 min

cutting speed of 90 m/min, it shows that the depth KT and width KB of crater wear increase along with time. When cutting continues from 7 to 12 min, the KT rises by 0.08 mm, and the KB is raised by 0.2 mm. In the meantime, the distance from the center of crake wear to the tip of the tool to remains stable, i.e., 0.1 mm. It bears a resemblance under other cutting speed to the cutting speed of 90 m/min. Along with the cutting process, the crater wear moves toward the tool tip, which deteriorates the strength of the tool and brings about the concentration of stress and tipping. Accordingly, the tool fails easily.

Moreover, as shown in Fig. 15, the crater morphology can be found under different cutting speed. The higher the speed, the shorter the time a cutting tool reaches the standard of wear dulling, and the cutting speed will also affect the distance between the center of the crater wear and the tip of the tool (KM). Although it does not change much, it can be seen that the larger the speed, the smaller the KM value, and the center of the crater will lean toward the cutting edge. When the speed is 120 m/min, KM is 0.12 mm, and when the speed increases to 300 m/min,

KM is reduced to 0.08 mm. The change of KM is accompanied by the change of KB value, which means that the center of the crater is tilted toward the tip of the blade, and the width of the crater is decreasing.

4.2.2 Impact of feed rate on tool wear

As shown in Fig. 16, for the speed of 120 m/min, depth of 1 mm, and the feed rate is 0.1 mm/r, 0.15 mm/r, and 0.2 mm/r respectively, the depth of KT value of the rack face of the tool is with the curve of the cutting time. As can be seen from the curve in Fig. 16, the increase of supply will speed up the tool wear, but its effect is much smaller than the cutting speed. When feed rate from 0.1 mm/r increases to 0.2 mm/r, the time used to reach wear dulling standard for the tool is reduced by less than 2 min. Therefore, it is suggested that the impact of feed rate on tool wear is much smaller than speed.

Under the same conditions, the depth of crater wear KT (on the rack face of the cemented carbide tool) against the time under the different feed rate is shown in Fig. 17. Figure 17

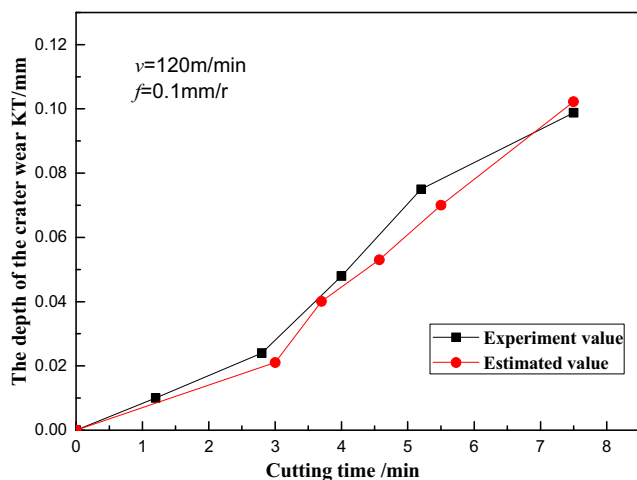


Fig. 12 Tool wear experimental results compared with the simulation results

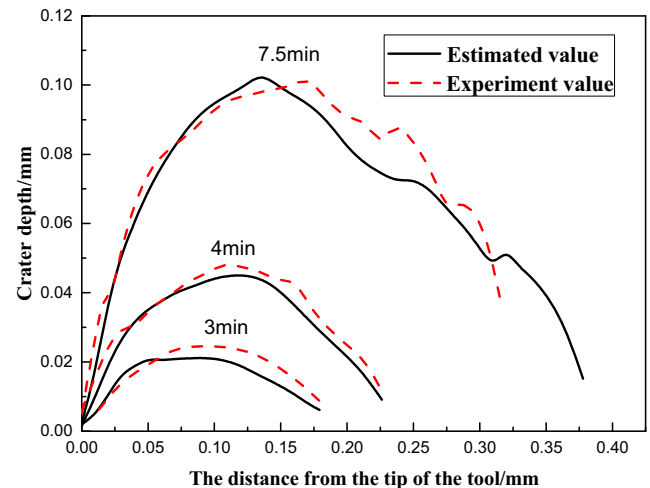


Fig. 13 The experiments and simulations of the rack face wear morphology of the tool are compared

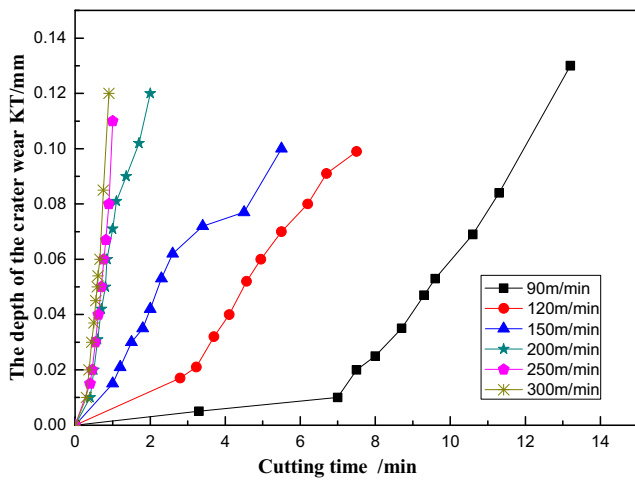


Fig. 14 Crater wear depth (KT) under the different speeds

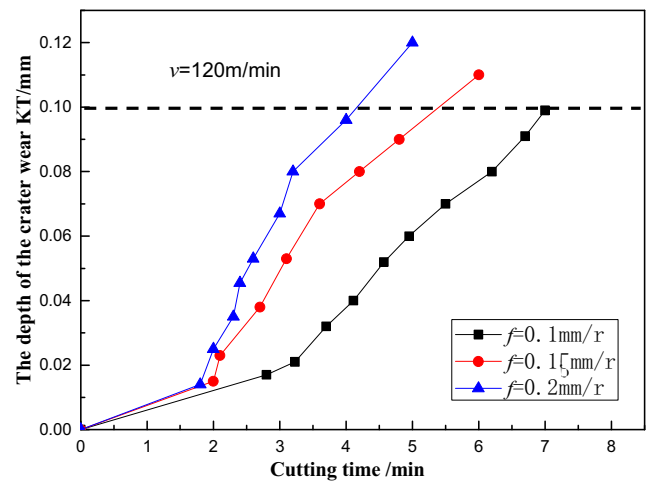


Fig. 16 The crater wear depth (KT) under different feed rates

shows that the depth KT and width KB of crater wear increase along with time. Along with the cutting process, the crater wear moves toward the tool tip, which deteriorates the strength of the tool and brings about the concentration of stress and tipping. Accordingly, the tool fails easily.

Similar to cutting speed, as shown in Fig. 17, the crater morphology can be found under different feed rates, the cutting speed will affect the distance between the center of the crater wear and the tip of the tool (KM). When the feed rate

increased from 0.1 to 0.2 mm/r, the KM value increased from 0.15 to 0.25 mm. The change of feed rate will directly affect the tool-chip contact length; the tool-chip contact length increases as the feed rate increases. This means that as feed rate increases, and the deepest point of the crater is farther from the tip of the tool. As is shown in Fig. 17, when the feed rate increased from 0.1 to 0.2 mm/r, the KB value increased from 0.375 to 0.47 mm, it can be seen that the width of the crater also increases with the increase of feed rate.

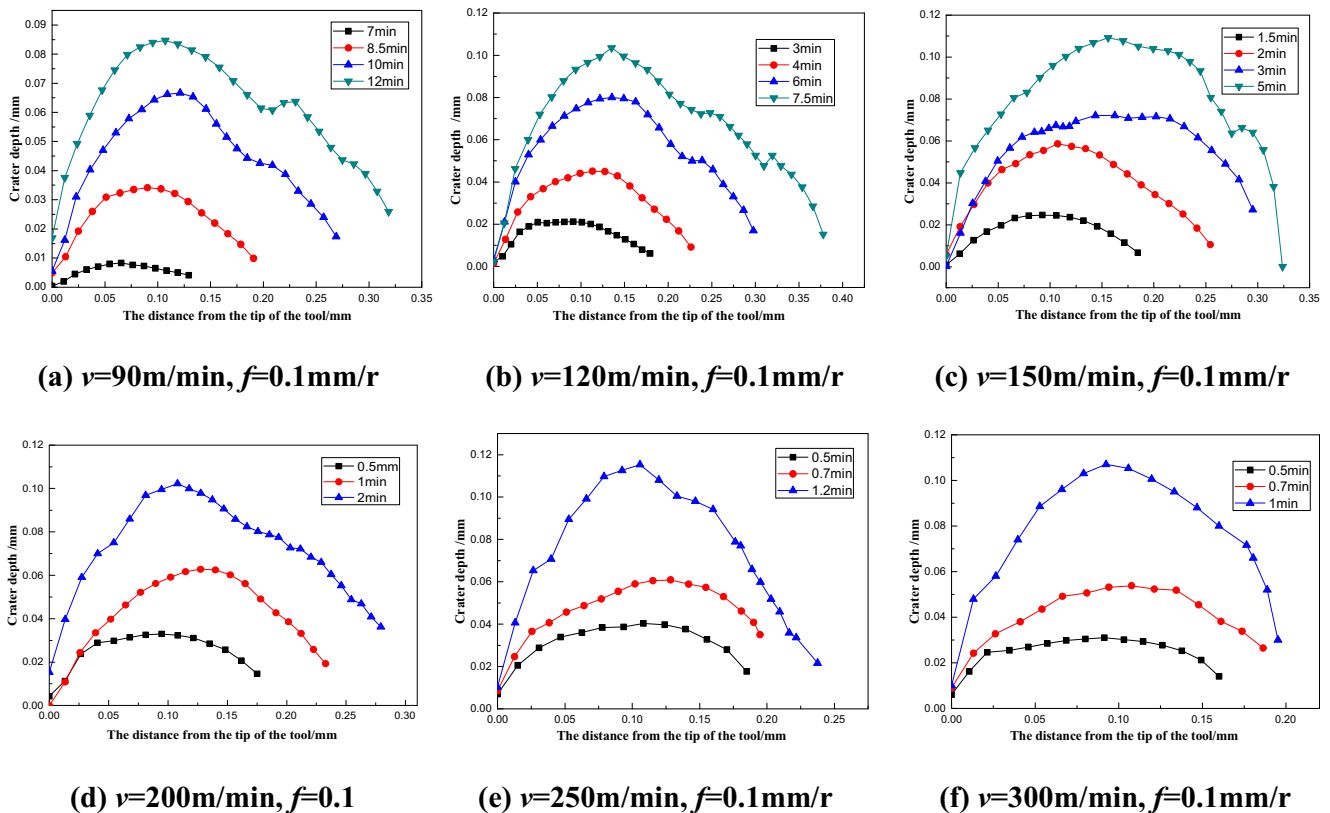


Fig. 15 The crater morphology under the different cutting speed **a** $v = 90$ m/min, $f = 0.1$ mm/r, **b** $v = 120$ m/min, $f = 0.1$ mm/r, **c** $v = 150$ m/min, $f = 0.1$ mm/r, **d** $v = 200$ m/min, $f = 0.1$, **e** $v = 250$ m/min, $f = 0.1$ mm/r, and **f** $v = 300$ m/min, $f = 0.1$ mm/r

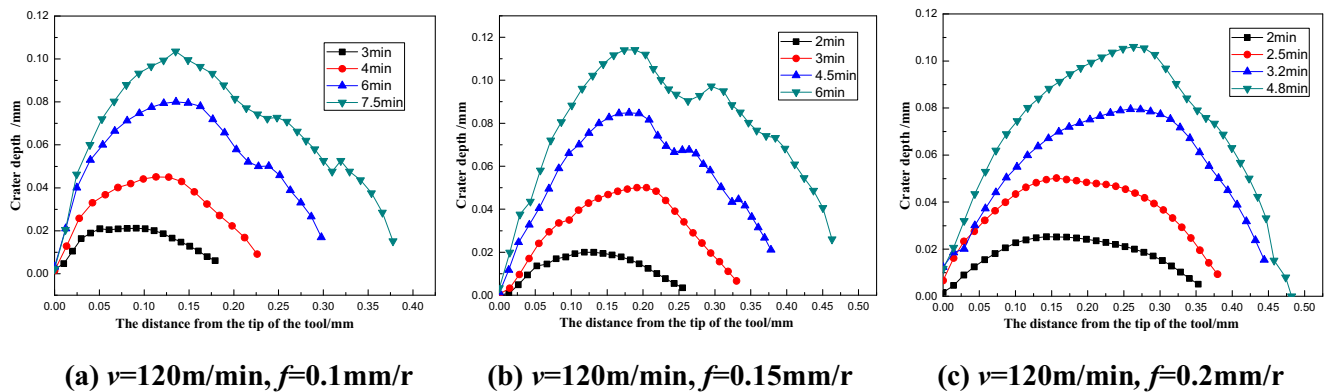


Fig. 17 The crater morphology under the different feed rates. **a** $v = 120$ m/min, $f = 0.1$ mm/r. **b** $v = 120$ m/min, $f = 0.15$ mm/r. **c** $v = 120$ m/min, $f = 0.2$ mm/r

4.3 The determination of the tool life

By analyzing the influence rule of different parameters on tool wear, the formula of tool life is:

$$T = \frac{C_T}{v^a f^b} \quad (5)$$

where T is the tool durability, v is the cutting speed, f is the feed quantity, C_T is the durability factor (related to cutting tools, workpiece materials and cutting conditions), and a and b are indices. By the linear fitting of the data from the results of the simulations (Figs. 15, 17), the formula a is 2.21, b is 0.63, and C_T is $e^{11.03}$.

Through comparison and analysis, the influence of different cutting parameters on tool wear and access to the tool life of formula shows that the effects of speed on tool wear effect are remarkable, and the feed rate for the influence of tool wear is relatively small. Because the simulation using the orthogonal cutting and the cooling way is dry cutting, the working condition is bad, and tool wear is faster. When cutting speed is lower than 200 m/min, the speed of tool wear is relatively smooth. Therefore, it is recommended that the reasonable parameter range of cemented carbide cutting tool in high-speed dry cutting Ti6Al4V is 90–150 m/min, and the feed rate is 0.10–0.20 mm/r.

5 Conclusion

In this paper, a novel finite element method for the wear analysis of cemented carbide tool during high-speed cutting Ti6Al4V alloy was proposed. The high-speed cutting tests were carried out on Ti6Al4V to verify the tool wear prediction FEM model. The main conclusions are as follows:

- (1) A novel technique has been introduced to update the geometry of the rake face of the cutting tool without the manual intervention of the numerical simulation.

This step is an inevitable condition for analyzing the tool wear geometry.

- (2) The reliable FEM model of tool wear is built that can consider various wear mechanisms (abrasive wear, adhesive wear, and diffusive wear) occurring in high-speed cutting Ti6Al4V process. The tool wear model, predicting the depth and width of tool wear at any given cutting conditions, was verified by experiments.
- (3) The influence of cutting speed and feed rate on the tool wear was predicted by the proposed FEM model. The significant impact of the feed rate on the tool life that is less than the impact of the cutting speed was observed. The influence of different machining parameters on tool wear morphology is analyzed. The reasonable parameter range of cemented carbide cutting tool in high-speed dry cutting Ti6Al4V is 90–150 m/min, and the feed rate is 0.10–0.20 mm/r.

Funding information The authors gratefully acknowledge the financial supports of the National Natural Science Foundation of China (No. 51275231), the Anhui Provincial Natural Science Foundation (NO. 1608085ME121), and Nanjing University of Aeronautics and Astronautics PhD short-term visiting scholar project (No. 190304DF06).

References

1. Sartori S, Taccin M, Pavese G, Ghiotti A, Bruschi S (2018) Wear mechanisms of uncoated and coated carbide tools when machining Ti6Al4V using LN2 and cooled N2. *Int J Adv Manuf Technol* 95: 1255–1264
2. Liu HG, Zhang J, Xua X, Zhao WH (2018) Experimental study on fracture mechanism transformation in chip segmentation of Ti-6Al-4V alloys during high-speed machining. *J Mater Process Technol* 257:132–140
3. Wu HB, Zhang SJ (2015) Effects of cutting conditions on the milling process of titanium alloy Ti6Al4V. *Int J Adv Manuf Technol* 77: 2235–2240
4. Ji CH, Li YH, Qin XD, Zhao Q, Sun D, Jin Y (2015) 3D FEM simulation of helical milling hole process for titanium alloy Ti-6Al-4V. *Int J Adv Manuf Technol* 81:1733–1742

5. Rosemar B, Machado ÁR (2013) Tool life and wear mechanisms in high speed machining of Ti–6Al–4V alloy with PCD tools under various coolant pressures. *J Mater Process Technol* 213:1459–1464
6. Kaplana B, Odelrosa S, Kritikosa M, Bejjania R, Norgrenab S (2018) Study of tool wear and chemical interaction during machining of Ti6Al4V. *Int J Refract Met Hard Mater* 72:253–256
7. Rahman Rashid RA, Palanisamy S, Sun S, Dargusch MS (2016) Tool wear mechanisms involved in crater formation on uncoated carbide tool when machining Ti6Al4V alloy. *Int J Adv Manuf Technol* 83:1457–1465
8. Fan YH, Hao ZP, Zheng ML, Yang SC (2016) Wear characteristics of cemented carbide tool in dry-machining Ti-6Al-4V. *Mach Sci Technol* 20(2):249–261
9. Yang YF, Su YS, Li L, He N, Zhao W (2015) Performance of cemented carbide tools with microgroove in Ti-6Al-4V titanium alloy cutting. *Int J Adv Manuf Technol* 76:1731–1738
10. Costes JP, Guillet Y, Poulachon G, Dessoly M (2007) Tool life and wear mechanisms of CBN tools in machining[J]. *Int J Mach Tool Manu* 47(7–8):1081–1087
11. Takeyama H, Murata (1963) Basic investigation of tool wear. *J Eng Ind Trans ASME* 85(1):33–38
12. Mathew P (1989) Use of predicted cutting temperatures in determining tool performance. *Int J Mach Tool Manu* 29(4):481–497
13. Attanasio A, Ceretti E, Fiorentino A, Cappellini C, Giardini C (2010) Investigation and FEM-based simulation of tool wear in turning operations with uncoated carbide tools. *Wear* 269:344–350
14. Umbrello D, Filice L (2009) Improving surface integrity in orthogonal machining of hardened AISI 52100 steel by modeling white and dark layers formation. *CIRP Ann Manuf Technol* 58(1):73–76
15. Buchkremer S, Klocke F, Lung D (2015) Finite-element-analysis of the relationship between chip geometry and stress triaxiality distribution in the chip breakage location of metal cutting operations. *Simul Model Pract Theory* 55:10–26
16. Zanger F, Schulze V (2013) Investigations on mechanisms of tool wear in machining of Ti-6Al-4V using FEM simulation. 14th CIRP conference on modeling of machining operations (CIRP CMMO), vol 8, pp 158–163
17. Altan T, Yen YC, Söhner J, Weule H, Schmidt J (2002) Estimation of tool wear of carbide tool in orthogonal cutting using FEM simulation. In: CIRP Int. workshop on modeling of machining operations, pp 149–160
18. Attanasio A, Ceretti E, Rizzuti S (2008) 3D finite element analysis of tool wear in machining[J]. *CIRP Ann Manuf Technol* 57:61–64
19. Filice L, Micari F, Settineri L, Umbrello D (2007) Wear modelling in mild steel orthogonal cutting when using uncoated carbide tools. *Wear* 262:545–554
20. Binder M, Klocke F, Doebbler B (2017) An advanced numerical approach on tool wear simulation for tool and process design in metal cutting. *Simul Model Pract Theory* 70:65–82
21. Fleischer J, Schmidt J, Xie L J, Schmidt C, Biesinger F (2004) 2D tool wear estimation using finite element method. In: Moisan A, Poulachon G (eds) Proceedings of the seventh CIRP international workshop on modeling of machining operations, Cluny, pp 82–91
22. Yen YC, Söhner J, Lilly B, Altan T (2004) Estimation of tool wear in orthogonal cutting using the finite element analysis. *J Mater Process Technol* 146:82–91
23. Kalhori V (2001) Modelling and simulation of mechanical cutting. PH.D thesis, The Polhem Laboratory Division of Computer Aided Design Department of Mechanical Engineering, Sweden
24. Chetan A, Narasimhulu S, Ghosh P, Rao V (2015) Study of tool wear mechanisms and mathematical modeling of flank wear during machining of Ti alloy (Ti6Al4V). *J Inst Eng (India)* 96(3):279–285
25. Cao ZY, He N, Li L (2008) A finite element analysis of micromeso-scale machining considering the cutting edge radius. *Appl Mech Mater* 11(12):631–636
26. Usui E, Shirakashi T (1984) Analytical prediction of cutting tool wear. *Wear* 100:129–151
27. Abukhshim NA, Mativenga PT, Sheikh MA (2006) Heat generation and temperature prediction in metal cutting: a review and implications for high speed machining. *Int J Mach Tool Manu* 46(7–8):782–800

Publisher's note Springer Nature remains neutral with regard to jurisdictional claims in published maps and institutional affiliations.